BINDING OF CYTOTOXIC Aβ25-35 PEPTIDE TO THE DMPC LIPID BILAYER

Amy K. Smith and Dmitri K. Klimov

School of Systems Biology, George Mason University, Manassas, VA 20110

E-mail: dklimov@gmu.edu

Supporting Information

Assessment of REST performance: The conformational ensemble of two Aβ25-35 peptides interacting with the DMPC bilayer was generated using replica exchange with solute tempering (REST) molecular dynamics simulations. These simulations used *R*=6 replicas distributed exponentially in the temperature range from 330K to 440K. To observe replica mixing across the temperature range, the walk of replicas over all temperatures for each production REST trajectory was visualized. A representative replica walk is displayed in Fig. S1, illustrating that no replica remains trapped at any temperature. Therefore, the figure exhibits efficient replica mixing across temperatures, which is a necessary condition for REST simulation convergence.

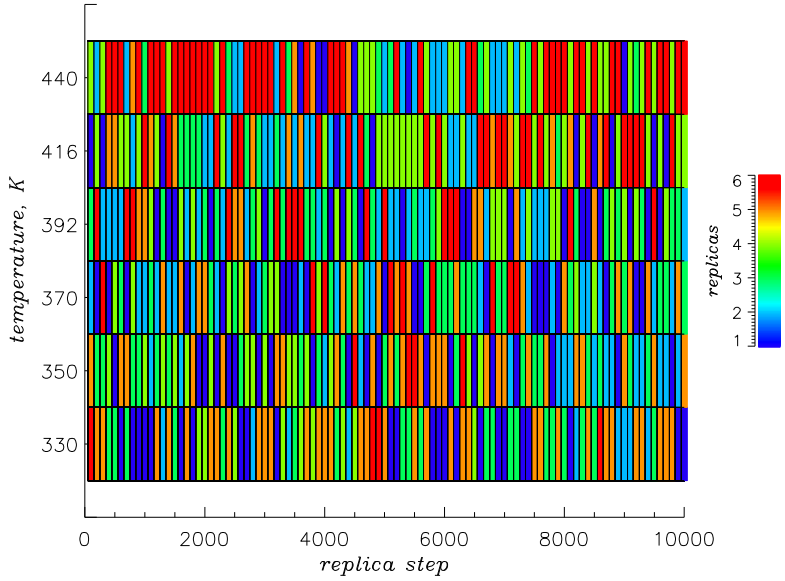

Figure S1. Random walk of replicas over temperatures in a representative production REST trajectory. The distribution of replicas over temperatures at the beginning of the trajectory is color-coded according to the scale. Emerging color mosaic suggests efficient replica mixing.

Another measure of replica mixing is the parameter proposed by Han and Hansmann [1]:

$$m(T) = 1 - \frac{\sqrt{\sum_{r=0}^{R-1} t_r^2}}{\sum_{r=0}^{R-1} t_r}, \qquad (1)$$

where T is the REST temperature and t_r is the total number of REST iterations spent at T by replica r. For R=6 the optimum theoretical value of m independent of temperature is $1 - 1/R^{1/2} = 0.59$. Fig. S2 presents $m(T)$ averaged over all production trajectories showing that this quantity approaches the theoretical value

at all REST temperatures. Some deviations at the edges of the temperature range occur due to boundary effects impacting random replica walk. Therefore, Fig. S2 indicates nearly ideal replica mixing.

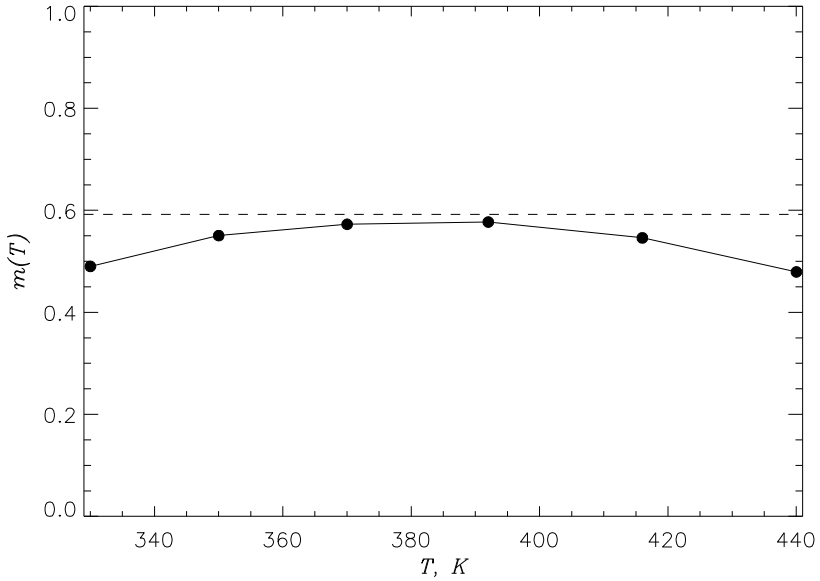

Figure S2. The mixing parameter $m(T)$ as a function of the REST temperature T. Dashed line indicates the optimum theoretical value of 0.59.

Our previous study [2] has also used another quantity to assess REST performance, namely, the average replica exchange rate $\alpha(T)$ at each REST temperature T. The rate $\alpha(T)$ is defined as the fraction of successful replica exchange attempts at a given REST temperature T. Fig. S3 displays $\alpha(T)$, from which we surmise that $\alpha(T)$ is consistent across all REST temperatures being approximately equal to 0.25.

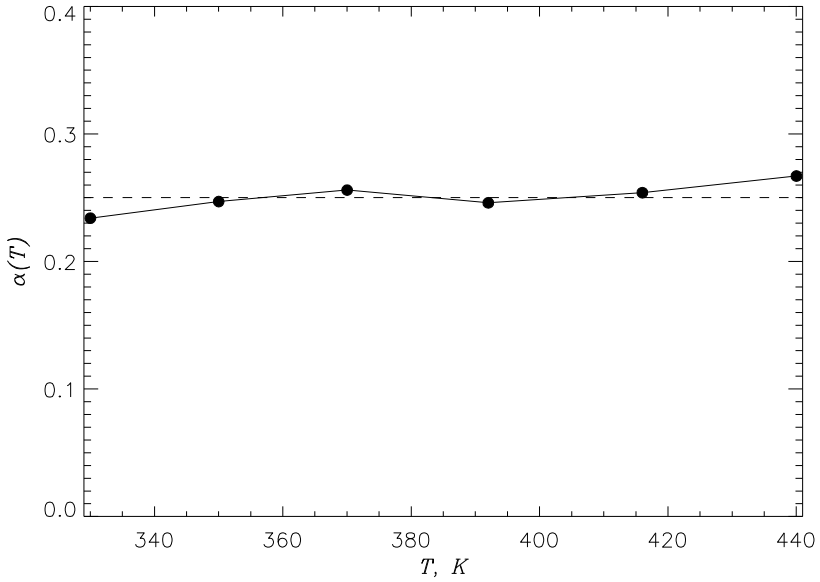

Figure S3. Average replica exchange rate $\alpha(T)$ computed for production REST simulations as a function of REST temperature T. The dashed line marks the value of $\alpha(T)$ averaged across all temperatures.

Conformational sampling in REST simulations: Equilibration of REST sampling was analyzed using preliminary (40 ns per replica) and production (20 ns per replica) stages of the six simulation trajectories

totaling in all 60 ns per replica in a trajectory. To assess equilibration we first monitored the probability distributions $P(z_{com})$ of the z-position of Aβ25-35 center of mass z_{com} along the DMPC bilayer normal averaging it over six trajectories. The corresponding plots for different equilibration times τ_{eq} are presented in Fig. S4a. Because the first overlapping $P(z_{com})$ occur after τ_{eq}=42 ns, we discarded initial 42 ns of sampling per replica in a trajectory. This equilibration length is shorter than τ_{eq} reported for antimicrobial peptide indolicidin [3]. The likely reasons for longer idolicidin τ_{eq} are that this peptide is highly cationic and its sampling was performed using umbrella method without replica exchange. In addition, we have considered the distribution of helix structure along Aβ25-35 sequence $<H(i)>$ as a function of τ_{eq}. Fig. S4b shows that this quantity equilibrates faster than $P(z_{com})$.

(a)

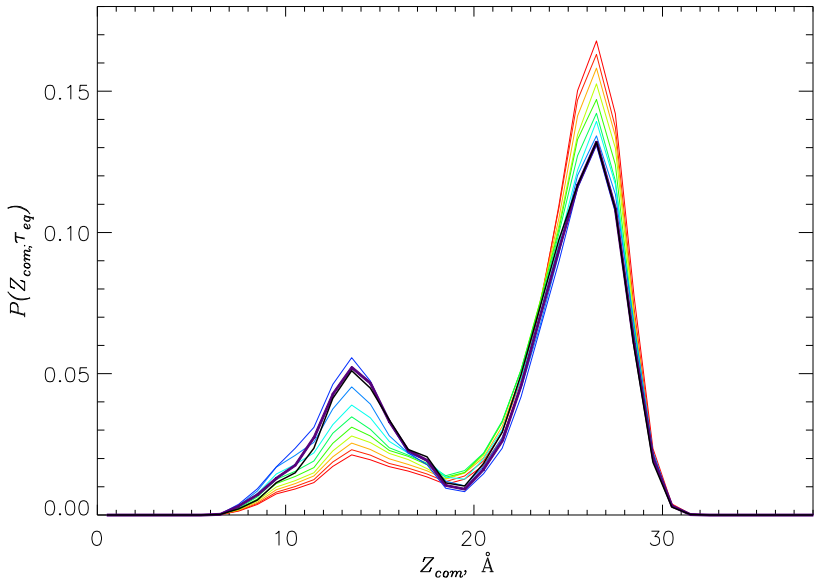

(b)

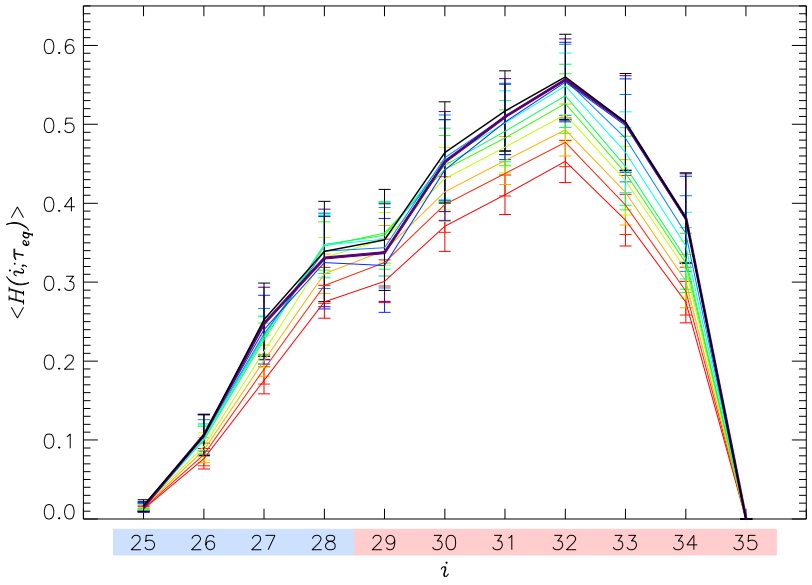

Figure S4. (a) Probability distributions $P(z_{com})$ of the z-position of Aβ25-35 center of mass z_{com} along the DMPC bilayer normal at different equilibration times τ_{eq} defined as the initial simulation time excluded from data collection in a 330K (r=0) replica in each trajectory. Thin red through blue lines represent $P(z_{com})$ collected with τ_{eq} from 0 to 40 ns with the increment of 5 ns. Thick purple and black lines correspond to τ_{eq} =42 and 44 ns. (b) Helix propensities for Aβ25-35 amino acids i, $\langle H(i) \rangle$, as a function of τ_{eq}.The line colors and their types follow (a). Sampling errors are shown by vertical bars.

The convergence of equilibrated REST simulations was evaluated using several measures. As performed in our previous studies [4], we first enumerated unique conformational states N_s collected as a function of the cumulative equilibrium simulation time τ_{sim}, i.e., elapsed in all trajectories in the wild-type replica (r = 0). Unique states were defined by their enthalpy H and a structural quantity X. Following our previous studies [4], we utilized as X the number of intrapeptide contacts C and the number of peptide-lipid contacts C_l. In addition, to probe the localization of Aβ25-35 in the bilayer, we defined N_s using as X the distance between the bilayer midplane and the peptide center of mass z_{com}. To bin H we used the interval of 2 kcal/mol, whereas for z_{com} we applied the interval of 1 Å. As the growth of N_s is affected by an arbitrary order, in which the simulation snapshots are processed, a set of 200 random permutations ordering the six independent trajectories was used to average $N_s(\tau_{sim})$. Accordingly, Fig. S5 displays the numbers of unique states N_s collected by the 330K wild-type REST replica (r = 0) as a function of τ_{sim}. This figure demonstrates approximate saturation in the number of unique states collected according to all three definitions, which is a prerequisite for sampling convergence. In fact, over the full range of τ_{sim} the slopes of $N_s(\tau_{sim})$ have decreased at least 30-fold.

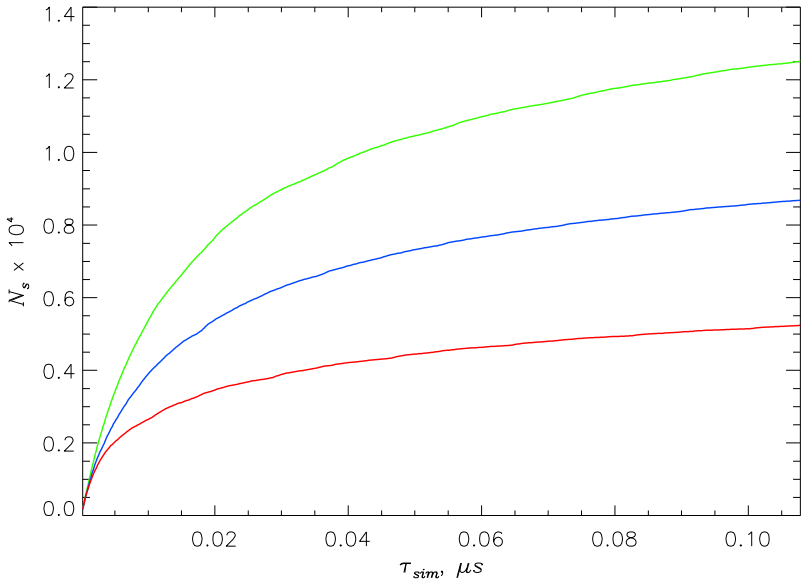

Figure S5. The numbers of unique states N_s collected at 330K as a function of cumulative equilibrium simulation time τ_{sim}. Green, blue, and red lines display N_s defined using (H,C_l), (H, z_{com}), and (H,C) states, respectively.

Second, we computed the probabilities of inserted I and surface-bound S states, $P(I)$ and $P(S)$, as a function of cumulative equilibrium simulation time τ_{sim}. Fig. S6 reveals initial drift of $P(I)$ and $P(S)$ followed by their eventual stabilization at τ_{sim}> 90 ns. The final values of $P(I)$ and $P(S)$ are 0.31±0.07 and 0.69±0.07. Note that the sampling errors are sufficiently small to clearly distinguish $P(I)$ and $P(S)$.

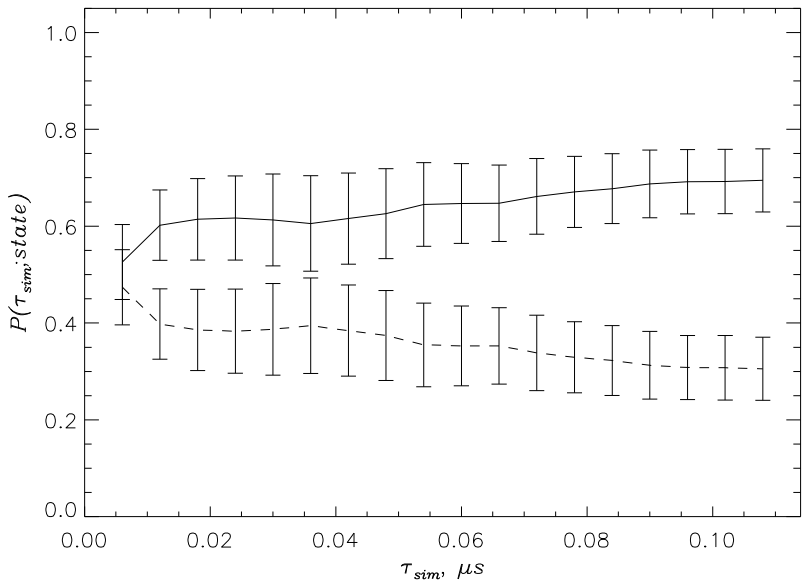

Figure S6. Probabilities of inserted I and surface-bound S states, *P(I)* (dashed line) and *P(S)* (solid line), as a function of cumulative equilibrium simulation time τ_{sim} at 330K. Vertical bars represent sampling errors.

Third, using entire equilibrium sampling at 330K we computed separately the average distances <*z(i)*> of amino acids *i* from the bilayer midplane for each of the two Aβ25-35 peptides. Fig. S7 shows a very good agreement between <*z(i)*> for both peptides, demonstrating that both Aβ25-35 peptides sample the same bilayer regions along the normal *z*. Taken together, we conclude that our REST simulations satisfy multiple measures of sampling convergence in Figs. S4-S7. Similar evidence of REST convergence has been observed in the control simulations of Aβ25-35 in lipid-free water.

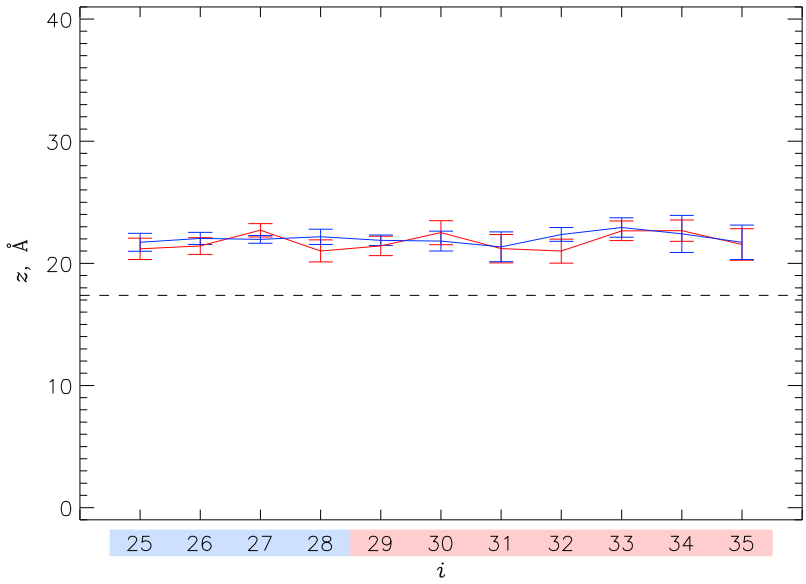

Figure S7. The average distances <*z*(*i*)> of the centers of mass of amino acids *i* to the bilayer midplane for each Aβ25-35 peptide (data in red and blue). Vertical bars represent sampling errors. The dashed line marks the average position of phosphorus atoms center of mass. Almost perfect overlap of two <*z*(*i*)> distributions suggests consistency in REST sampling between the two peptides.

Impact of bilayer restraints: To prevent lipid escape from the bilayer, we harmonically restrained the position of the center of mass of phosphorous P atoms in each leaflet. In our previous paper [5] we have evaluated the impact of such restraints on bilayer properties. Specifically, we compared the order parameter $\langle S_{CD}(i) \rangle$ and the dipolar coupling parameter $\langle \Delta\nu_D \rangle$ computed for the DMPC bilayers with and without restraints and found that their respective values coincide within the sampling error. We also computed the areas per lipid $\langle A_l \rangle$ for the bilayers with and without restraints and found them to be in good agreement (65.1 ± 0.0 and 64.9 ± 0.3 Å^2, respectively). In another study we have shown that the restraints introduce minor differences between the lipid structural properties in the distant region of the bilayer with bound Aβ peptides and in the Aβ-free bilayer [6]. Therefore, we believe that the impact of these harmonic restraints is insignificant.

Interactions with the DMPC bilayer: To explore the differences in the binding energetics between Aβ25-35 and Aβ25-35(10-40), we decompose peptide-lipid contacts into those formed by apolar, polar, and cationic amino acids. The numbers of contacts with lipids $\langle C_l \rangle$ attributed to each of these amino acids types are presented in Table S1 and their implications are discussed in the main text.

Table S1 Binding contacts between Aβ peptides and lipids

Amino acid type	Aβ25-35	Aβ25-35(10-40)
apolar	7.5±0.9	9.2±2.3
polar	3.3±0.2	2.9±0.7
cationic	1.6±0.2	0.4±0.1
all	12.3±1.1	12.5±3.1

Impact of Aβ25-35 binding on the DMPC bilayer distant region: It is important to comment on the following question: To which extent does the distant region of the bilayer resemble the Aβ-free DMPC bilayer? We have explored this question in our previous paper [5] by systematically comparing the distant region of the DMPC bilayer with the bound Aβ10-40 peptide to the Aβ-free DMPC bilayer. Specifically, we computed (i) surface lipid number density, (ii) the area per lipid, (iii) the bilayer thickness defined as the distance between phosphorous (P) atoms centers of mass, (iv) the P-P radial number density distribution function, (v) the order parameters S_{CD} and S_{CC} probing the orientation of fatty acid C-H and C-C bonds, and (vi) the tilt and lengths of DMPC fatty acid tails. These quantities showed either perfect match or differences not exceeding 6%. Because our Aβ25-35 simulations use the DMPC bilayer of the same size as in [5], (ii) the radius of Aβ25-35 binding footprint R_c is smaller than of Aβ10-40, and (iii) Aβ25-35 does not penetrate the bilayer as deep as Aβ10-40, we believe that Aβ25-35 peptide induces minor perturbations to the distant bilayer region.

Aβ25-35 two-state analysis: In the main text, we describe in detail the two peptide conformational ensembles observed upon binding to the DMPC bilayer: the inserted (I) and surface-bound (S) peptide states. Their conformational properties are illustrated in Fig. S8.

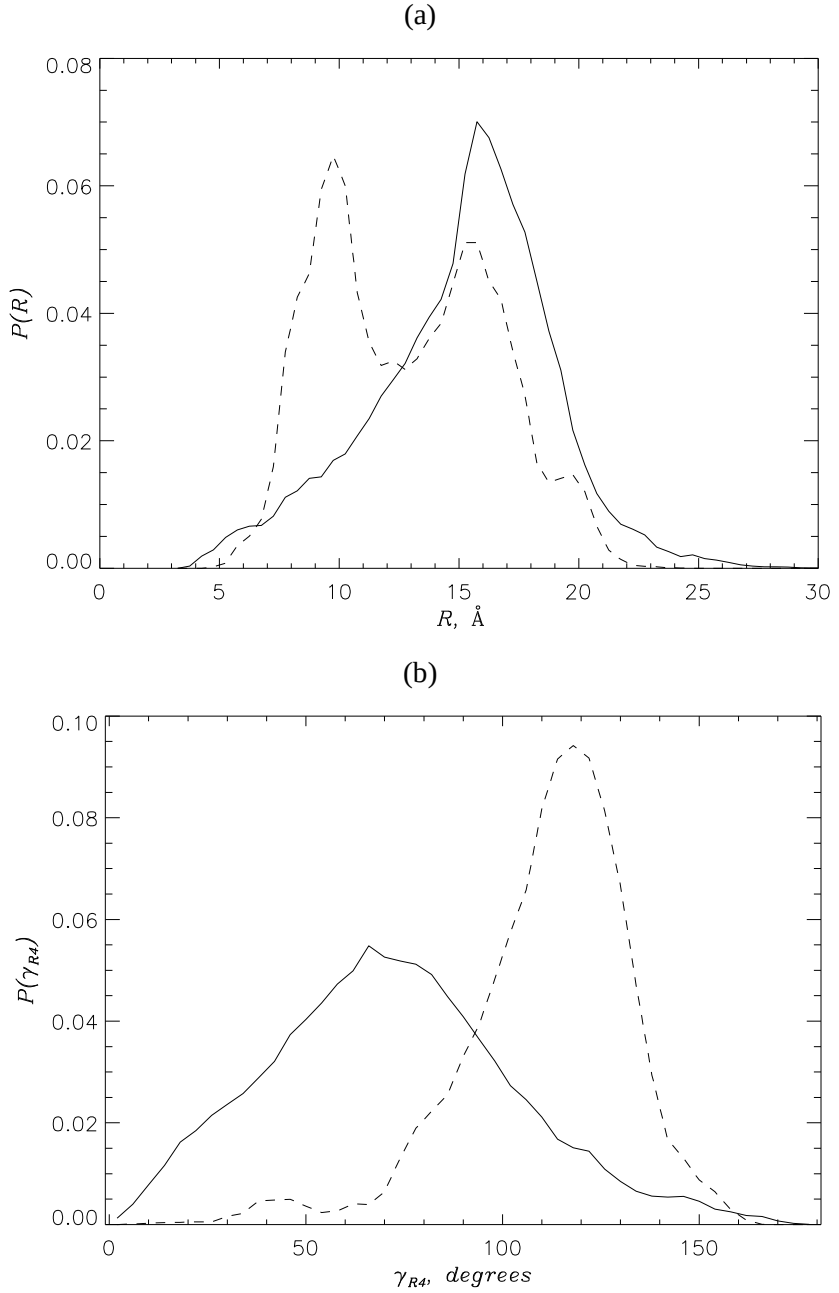

Figure S8 (a) Probability distributions *P(R)* of the Aβ25-35 end-to-end distance *R* for the S (solid line) and I (dashed line) states. (b) Probability distributions $P(\gamma_{R4})$ of the tilt angle of Aβ25-35 C-terminal R4 with respect to the bilayer normal γ_{R4} computed for the S (solid line) and I (dashed line) states. According to these panels the peptide in the S state adopts extended conformation with the C-terminal pointed away from the bilayer surface. The peptide in the I state has more compact structure with the C-terminal directed toward the bilayer.

The energetics of the two Aβ25-35 bound states is presented in Table S2. It shows that the total non-bonded interaction energy between the peptide and its environment is lower for the state S compared to

the state I. We also present in Table S2 the contributions of electrostatic and van der Waals interactions to these energies, and we decompose the interactions into bilayer and solvent (water and ions) contributions. It is seen that the electrostatic interactions between the peptide and solvent provide the greatest contribution to binding energy in both states. As expected this electrostatic interaction energy is the most favorable in the state S. Furthermore, in the state I the bilayer provides most of van-der-Waals interactions, whereas in the state S the largest contribution to van-der-Waals energy comes from water.

Table S2. Energetics of the inserted I and surface bound S states.

State	Peptide interacting with	Electrostatic interaction energy (kcal/mol)	VDW interaction energy (kcal/mol)	Total energy (kcal/mol)
I	bilayer	-111.4	-62.8	-368.2
	solvent	-175.5	-18.9	
S	bilayer	-68.0	-14.1	-381.4
	solvent	-246.9	-52.4	

Water permeation: We have considered the possibility that binding of Aβ25-35 monomers to the DMPC bilayer promotes water invasion into the bilayer core. To this end, we have computed the water number density $n_w(r,z)$ as a function of the distance r to Aβ25-35 center of mass and the distance z to the bilayer midplane. Fig. S9 compares $n_w(r,z)$ between distant and proximal regions of the DMPC bilayer for Aβ25-35 peptides adopting surface-bound and inserted states. The figure shows that neither of Aβ25-35 bound states facilitate noticeable water incursion into the bilayer interior.

(a)

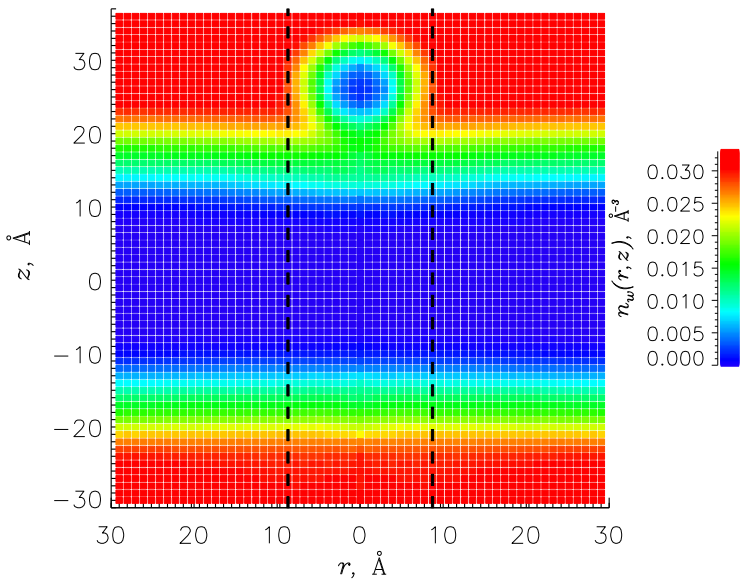

(b)

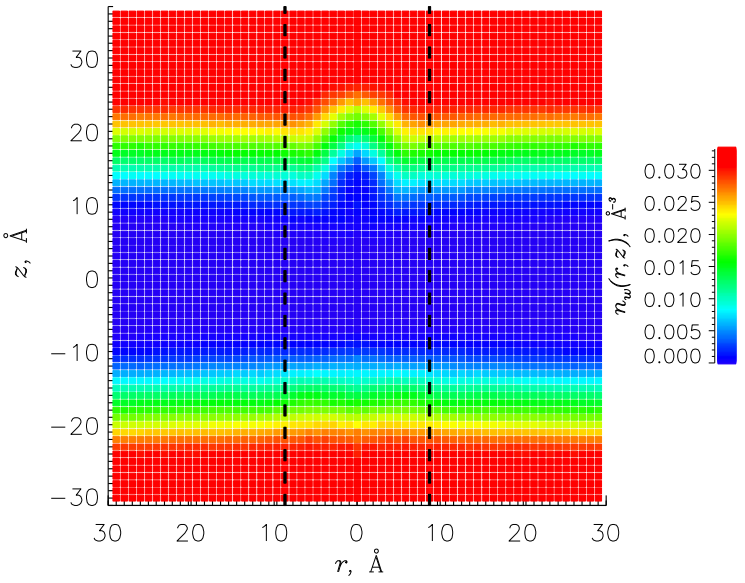

Figure S9 The cross-sectional number densities of water oxygen atoms $n_w(r,z)$ as a function of the distance r to the peptide center of mass and the distance z to the bilayer midplane. Panels (a) and (b) represent surface-bound and inserted Aβ25-35 states, respectively. Dashed lines separate proximal and distant bilayer regions. The figure suggests that neither S nor I Aβ25-35 states induce water invasion into the DMPC bilayer.

[1] Han, M. and Hansmann, U. H. E. (2011) Replica exchange molecular dynamics of the thermodynamics of fibril growth of Alzheimer's Aβ42 peptide. *J. Chem. Phys.* **135**, 065101.

[2] Parikh, N. and Klimov, D. K. (2017) Inclusion of lipopeptides into the DMPC lipid bilayer prevents Abeta peptide insertion. Phys. Chem. Chem. Phys., **19**, 10087-10098.

[3] Neale, C., Hsu, J. C. Y., Yip, C. M., and Pomès, R. (2014) Indolicidin binding induces thinning of a lipid bilayer. *Biophys. J.* **106**, L29-L31.

[4] Lockhart, C. and Klimov, D. K. (2016) The Alzheimer's disease Aβ peptide binds to the anionic DMPS lipid bilayer. *Biochim. Biophys. Acta* **1858**, 1118–1128.

[5] Lockhart, C. and Klimov, D. K. (2014) Binding of Aβ peptide creates lipid density depression in DMPC bilayer. *BBA Biomembranes* **1838**, 2678-2688.

[6] Lockhart, C. and Klimov, D.K. (2016) The Alzheimer's Disease Abeta Peptide Binds to the Anionic DMPS Lipid Bilayer. *BBA Biomembranes* **1858**, 1118–1128.